Composite Structures 134 (2015) 1036–1043

Contents lists available at ScienceDirect

Composite Structures

journal homepage: www.elsevier.com/locate/compstruct

Vibration analysis of functionally graded carbon nanotube-reinforced composite nanoplates using Mindlin's strain gradient theory

B. shahriari [a], M.R. Karamooz Ravari [b], H. Zeighampour [c,*]

[a] Department of Mechanical and Aerospace Engineering, Malek-Ashtar University of Technology, Isfahan 84145-115, Iran
[b] Department of Mechanical Engineering, Graduate University of advanced Technology, Kerman 76311-33131, Iran
[c] Faculty of Engineering, Shahrekord University, Shahrekord, Iran

ARTICLE INFO

Article history:
Available online 12 September 2015

Keywords:
FG-CNTRC nanoplate
Third order shear deformation theory
Mindlin's strain gradient theory
Size parameter

ABSTRACT

In this paper, vibrations of functionally graded carbon nanotube-reinforced composite (FG-CNTRC) nanoplates are investigated. In doing so, the third order shear deformation theory is used and the size parameter is taken into consideration by using Mindlin's strain gradient theory. Equations of FG-CNTRC nanoplates motion with partial differentials are derived from Hamilton's principle. Mechanical properties of the FG-CNTRC nanoplates are determined using the rule of mixture. Here, the FG-CNTRC nanoplate is modeled as simply supported and the Navier solution is used to solve the vibration problem. The results of the new model are compared with those of the classical model, which leads to the conclusion that the classical model is a special case of the Mindlin's strain gradient theory. More results show that the rigidity of the FG-CNTRC nanoplates in the Mindlin's strain gradient theory is more than that in the classical theory, which leads to an increase in natural frequencies. Moreover, in the present study, the effect of the manner of distribution of Carbon nanotubes (CNTs) in the nanoplate and the effect of the volume fraction of the CNTs on the vibration of the FG-CNTRC nanoplates is investigated.

1. Introduction

Thanks to their unique electrical, chemical and mechanical properties, carbon nanotubes (CNTs) have extensive application for electromechanical systems and for making composites. Nanostructures are used to reinforce polymer nanoplates [1,2]. Because of the small size of functionally graded carbon nanotube-reinforced composite (FG-CNTRC) nanoplates, it is difficult and time-consuming to study the mechanical properties of such components with common methods. For this reason, other methods such as experimental methods and continuum theories are used. Given the fact that the experimental method is costly and time-consuming, it is not economical. Therefore, researchers have recently attempted to use higher order continuum theories which are highly capable and easy to use [3,4]. Also, the nonlocal theory is used to study nanostructures. In the nonlocal theory, unlike in classical continuum theories, stress at one point is a function of strain at other points too [5–10].

Here, it should be noted that when converting the macroscale into micro/nanoscale, dependency of material properties is in the nanoscale, and, to take this phenomenon into consideration, this study uses Mindlin's strain gradient theory. On the other hand, it could be argued that because the study of FG-CNTRC nanoplates is in the nanoscale, use of the classical theory cannot predict the mechanical properties of FG-CNTRC nanoplates with great precision. Hence, higher order continuum theories [11–14] which take the size parameters into account are used.

In recent years, many researchers have attempted to investigate the mechanical and static behavior of FG-CNTRC beams and FG-CNTRC plates. Ke et al. investigated the nonlinear vibration of a FG-CNTRC beam. For this purpose, they used the Timoshenko beam and studied the effects of volume fraction and the manner of distribution of the CNT on the vibrational frequency [15]. Yas and Samadi investigated the vibration and buckling of the FG-CNTRC beam on elastic foundation and demonstrated that increase in the foundation stiffness leads to increase in critical load and natural frequency [16]. Shen et al. calculated the deformation of a FG-CNTRC plate for the volume fraction and the manner of distribution of CNTs and considered the effect of temperature in this model [17]. Lei et al. computed the nonlinear deformation of a CNTRC plate using the kp-Ritz method and examined the effect of volume fraction and the manner of distribution of CNTs on the deformation of this plate [18]. Lei et al. computed the buckling of a FG-CNTRC plate using the first order plate theory (FSDT) and

* Corresponding author.
E-mail addresses: shahriari@mut-es.ac.ir (B. shahriari), mrkaramoozravari@gmail.com (M.R. Karamooz Ravari), h.zeighampour@yahoo.com (H. Zeighampour).

http://dx.doi.org/10.1016/j.compstruct.2015.08.118
0263-8223/

demonstrated that increase in the volume fraction of this CNT is accompanied by increase in the buckling of the plate [19]. Alibeigloo investigated the static behavior of a FG-CNTRC plate located between two piezoelectric plates and computed the stress variation in the plate for different volume fractions of the CNTs [20]. Zhu et al. investigated the vibrational and static behavior of a FG-CNTRC plate using the first order shear deformable theory. To compute the frequency and deformation, they used the finite element method [21]. Shahrbabaki et al. studied the free vibration of a FG-CNTRC plate with different boundary conditions. He used the Ritz method to compute the frequencies and demonstrated that this plate has the highest frequency with clamped–clamped support [22].

To the best of knowledge of the authors of the present study, researchers have paid scant attention to the investigation of FG-CNTRC nanoplates using Mindlin's strain gradient theory. This paper investigates the effect of the size parameter on the free vibration of FG-CNTRC nanoplate. For this purpose, the equations governing the problem and the boundary conditions are derived using the Hamilton principle and by considering the formulation derived, the vibrations of FG-CNTRC nanoplates with simply supported boundary conditions are solved. The Navier procedure is used to solve the vibration problem. In the end, the effect of size parameter, volume fraction of the CNT and the manner of distribution of the CNTs in the FG-CNTRC nanoplate on the FG-CNTRC nanoplate vibration is studied.

2. Preliminaries

2.1. Mindlin's strain gradient theory

In recent years, higher order continuum theories have been used in the studies of nano/microstructures because they take the size parameter into consideration. The strain energy in higher order elasticity theories is dependent on strain and strain gradient [23–26]. Higher order continuum theories fall into the two categories of strain gradient theory and couple stress theory. In coupe stress theories, the higher order rotation gradient is taken into consideration in deformation equations. Mindlin rewrote the higher order stress theory which takes strain gradient into account [27]. He rewrote the equations for isotropic objects symmetric to the center. In this state, strain energy has five linear elastic constants in which the size parameter is considered. Mindlin's strain gradient theory incorporates a new set of equilibrium equations as well as classical equilibrium equations in which the size parameter is taken into account, too. In this theory, Aifantis simplified the Mindlin's strain gradient theory and replaced the five parameters with a single one [28]. The structural equations in this theory are expressed as:

$$\sigma_{ij} = C_{ijkl}(1 - l^2\nabla^2)\varepsilon_{kl}, \tag{1}$$

where l is the size parameter. Also, σ_{ij}, ε_{kl}, C_{ijkl} and ∇^2 are the stress tensors and strain tensors, fourth-order linear elastic material tensor and Laplacian operator, respectively.

2.2. Displacement field in the FG-CNTRC nanoplates

Fig. 1 displays three types of FG-CNTRC nanoplates, where the CNTs are distributed along the direction of nanoplate thickness.

The displacement field of the third order shear deformation theory (TSDT) can be written as [29]:

$$u(x,\theta,z,t) = U(x,\theta,t) + z\psi_x - c_1 z^3\left(\psi_x + \frac{\partial w}{\partial x}\right),$$

$$v(x,\theta,z,t) = V(x,\theta,t) + z\psi_y - c_1 z^3\left(\psi_y + \frac{\partial w}{\partial y}\right),$$

$$w(x,\theta,z,t) = W(x,\theta,t), \tag{2}$$

in which, U, V and W stand for the displacement vector in the middle surface of the CNTRC nanoplate, respectively; and t represents time. Also, ψ_x and ψ_θ are rotation around the x and θ axes. Also, $(c_1 = 4/3h^2)$.

2.3. TSDT formulation by using Mindlin's strain gradient theory

In this section, equations of motion of the nanoplate are derived using Mindlin's strain gradient theory. First, the classical strains are determined based on the displacement field in Eq. (2) as follows:

$$\begin{Bmatrix}\varepsilon_{xx}\\ \varepsilon_{yy}\\ \gamma_{xy}\end{Bmatrix} = \begin{Bmatrix}\varepsilon^{(0)}_{xx}\\ \varepsilon^{(0)}_{yy}\\ \gamma^{(0)}_{xy}\end{Bmatrix} + z\begin{Bmatrix}\varepsilon^{(1)}_{xx}\\ \varepsilon^{(1)}_{yy}\\ \gamma^{(1)}_{xy}\end{Bmatrix} + z^3\begin{Bmatrix}\varepsilon^{(3)}_{xx}\\ \varepsilon^{(3)}_{yy}\\ \gamma^{(3)}_{xy}\end{Bmatrix},$$

$$\begin{Bmatrix}\gamma_{yz}\\ \gamma_{xz}\end{Bmatrix} = \begin{Bmatrix}\gamma^{(0)}_{yz}\\ \gamma^{(0)}_{xz}\end{Bmatrix} + z^2\begin{Bmatrix}\gamma^{(2)}_{yz}\\ \gamma^{(2)}_{xz}\end{Bmatrix}, \tag{3}$$

$$\begin{Bmatrix}\varepsilon^{(0)}_{xx}\\ \varepsilon^{(0)}_{yy}\\ \gamma^{(0)}_{xy}\end{Bmatrix} = \begin{Bmatrix}\frac{\partial U}{\partial x}\\ \frac{\partial V}{\partial y}\\ \frac{\partial U}{\partial y} + \frac{\partial V}{\partial x}\end{Bmatrix}, \quad \begin{Bmatrix}\varepsilon^{(1)}_{xx}\\ \varepsilon^{(1)}_{yy}\\ \gamma^{(1)}_{xy}\end{Bmatrix} = \begin{Bmatrix}\frac{\partial \psi_x}{\partial x}\\ \frac{\partial \psi_y}{\partial y}\\ \frac{\partial \psi_x}{\partial y} + \frac{\partial \psi_y}{\partial x}\end{Bmatrix},$$

$$\begin{Bmatrix}\varepsilon^{(3)}_{xx}\\ \varepsilon^{(3)}_{yy}\\ \gamma^{(3)}_{xy}\end{Bmatrix} = -c_1\begin{Bmatrix}\frac{\partial \psi_x}{\partial x} + \frac{\partial^2 W}{\partial x^2}\\ \frac{\partial \psi_y}{\partial y} + \frac{\partial^2 W}{\partial y^2}\\ \frac{\partial \psi_x}{\partial y} + \frac{\partial \psi_y}{\partial x} + 2\frac{\partial^2 W}{\partial x \partial y}\end{Bmatrix}, \tag{4}$$

$$\begin{Bmatrix}\gamma^{(0)}_{yz}\\ \gamma^{(0)}_{xz}\end{Bmatrix} = \begin{Bmatrix}\psi_y + \frac{\partial W}{\partial y}\\ \psi_x + \frac{\partial W}{\partial x}\end{Bmatrix}, \quad \begin{Bmatrix}\gamma^{(2)}_{yz}\\ \gamma^{(2)}_{xz}\end{Bmatrix} = -c_2\begin{Bmatrix}\psi_y + \frac{\partial W}{\partial y}\\ \psi_x + \frac{\partial W}{\partial x}\end{Bmatrix}. \tag{5}$$

In the above equations, $(c_1 = 4/3h^2)$, $(c_2 = 3c_1)$.

Afterwards, considering the assumption of plain stress, the structural equations in the third order orthotropic plate are derived as:

$$\begin{Bmatrix}\sigma_{xx}\\ \sigma_{\theta\theta}\\ \sigma_{x\theta}\\ \sigma_{zx}\\ \sigma_{z\theta}\end{Bmatrix} = \begin{bmatrix}C_{11} & C_{12} & 0 & 0 & 0\\ C_{12} & C_{22} & 0 & 0 & 0\\ 0 & 0 & C_{33} & 0 & 0\\ 0 & 0 & 0 & C_{44} & 0\\ 0 & 0 & 0 & 0 & C_{55}\end{bmatrix}\begin{Bmatrix}\varepsilon_{xx}\\ \varepsilon_{\theta\theta}\\ 2\varepsilon_{x\theta}\\ 2\varepsilon_{zx}\\ 2\varepsilon_{z\theta}\end{Bmatrix}, \tag{6}$$

where, the elastic constants defined as:

$$C_{11} = \frac{E_{11}}{1 - \nu_{12}\nu_{21}}, \quad C_{22} = \frac{E_{22}}{1 - \nu_{12}\nu_{21}}, \quad C_{12} = \frac{\nu_{21}E_{11}}{1 - \nu_{12}\nu_{21}},$$
$$C_{33} = G_{12}, \quad C_{44} = G_{13}, \quad C_{55} = G_{23}, \quad G_{13} = G_{12}, G_{23} = 1.2G_{12}. \tag{7}$$

In Eq. (7) above, E_{11} and E_{22} are the effective Young's modulus of the FG-CNTRC nanoplate, G_{12}, G_{13} and G_{23} are the shear modulus, and ν_{12} and ν_{21} are Poisson's ratio. These parameters, using the rule of mixture, are as follows:

$$E_{11} = \eta_1 V_{CNT} E^{CNT}_{11} + V_m E^m, \tag{8}$$

$$\frac{\eta_2}{E_{22}} = \frac{V_{CNT}}{E^{CNT}_{22}} + \frac{V_m}{E^m}, \tag{9}$$

$$\frac{\eta_3}{G_{12}} = \frac{V_{CNT}}{G^{CNT}_{12}} + \frac{V_m}{G^m}, \tag{10}$$

In Eqs. (8)–(10) above, E^{CNT}_{11} and E^{CNT}_{22} stand for Young's modulus of the CNTs in longitudinal and transverse directions, respectively, and G^{CNT}_{12} represents the shear modulus of the CNTs. E^m and G^m are

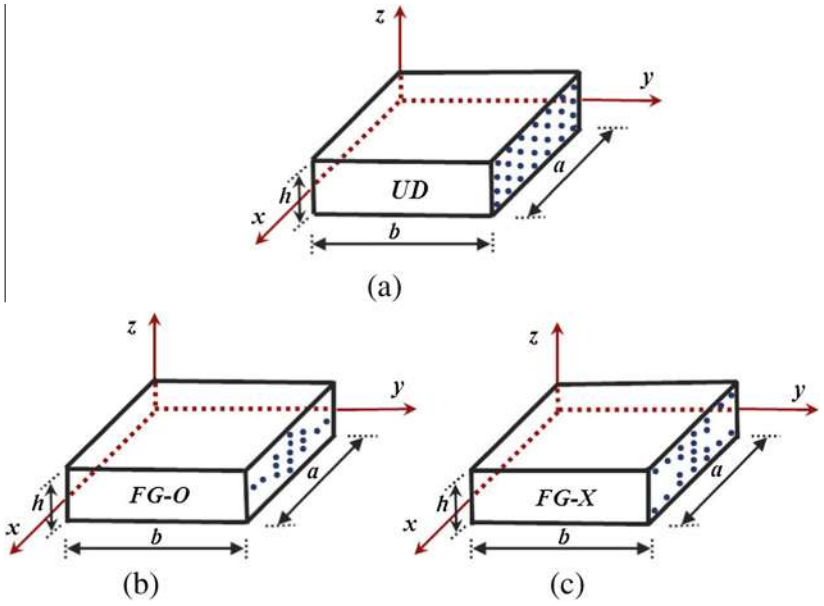

Fig. 1. Coordinates of CNTRC nanoplate.

Young's modulus and shear modulus of the isotropic matrix and $\eta_i (i = 1, 2, 3)$ is the CNT efficiency parameters. Poisson's ratio v_{12} is determined through the following equation:

$$\upsilon_{12} = \bar{V}_{CNT}\upsilon_{12}^{CNT} + V_m\upsilon^m, \tag{11}$$

In the above equations, V_{CNT} and $\bar{V}_{CNT}$ are the volume fractions of the CNTs which are divided into four categories based on the manner in which the CNTs are distributed along thickness [21].

$$\begin{aligned} V_{CNT}(z) &= \bar{V}_{CNT} \quad (\text{UD CNTRC}),\\ V_{CNT}(z) &= \left(\frac{4|z|}{h}\right)\bar{V}_{CNT} \quad (\text{FG}-\text{X CNTRC}),\\ V_{CNT}(z) &= 2\left(1-\frac{2|z|}{h}\right)\bar{V}_{CNT} \quad (\text{FG}-\text{O CNTRC}). \end{aligned} \tag{12}$$

Strain and kinetic energies are as follow:

$$U = \frac{1}{2}\int_{\Omega}(\sigma_{xx}\varepsilon_{xx} + \sigma_{yy}\varepsilon_{yy} + \sigma_{xz}\gamma_{xz} + \sigma_{xy}\gamma_{xy} + \sigma_{zy}\gamma_{zy})d\bar{V}, \tag{13}$$

$$T = \frac{1}{2}\int_0^b\int_0^a\int_{-h/2}^{h/2}\rho\left\{\left(\frac{\partial u}{\partial t}\right)^2 + \left(\frac{\partial v}{\partial t}\right)^2 + \left(\frac{\partial w}{\partial t}\right)^2\right\}dzdxdy. \tag{14}$$

In Eq. (14), density is as follows:

$$\rho = V_{CNT}\rho^{CNT} + V_m\rho^m. \tag{15}$$

By substituting the stresses from Eqs. (1) and (6) and strains (3)–(5) into Eq. (13) the strain energy is determined. The kinetic energy is determined by substituting the displacement. Equations of motion are obtained using the strain energy, kinetic energy and Hamilton's principle.

$$\begin{aligned} &A_1\frac{\partial^2 U}{\partial x^2} + A_2\frac{\partial^4 U}{\partial x^4} + A_3\frac{\partial^4 U}{\partial x^2\partial\theta^2} + A_4\frac{\partial^2 U}{\partial y^2} + A_5\frac{\partial^4 U}{\partial y^4} + A_6\frac{\partial^2 V}{\partial x\partial y} + A_7\frac{\partial^2 V}{\partial x^3\partial y}\\ &+ A_8\frac{\partial^4 V}{\partial x\partial y^3} + A_9\frac{\partial^5 W}{\partial x^5} + A_{10}\frac{\partial^3 W}{\partial x\partial y^2} + A_{11}\frac{\partial^5 W}{\partial x^3\partial y^2} + A_{12}\frac{\partial^3 W}{\partial x^3}\\ &+ A_{13}\frac{\partial^5 W}{\partial x\partial y^4} + A_{14}\frac{\partial^2\psi_x}{\partial x^2} + A_{15}\frac{\partial^4\psi_x}{\partial x^4} + A_{16}\frac{\partial^4\psi_x}{\partial x^2\partial y^2} + A_{17}\frac{\partial^2\psi_x}{\partial y^2}\\ &+ A_{18}\frac{\partial^2\psi_y}{\partial x\partial y} + A_{19}\frac{\partial^4\psi_x}{\partial y^4} + A_{20}\frac{\partial^4\psi_y}{\partial x^3\partial y} + A_{21}\frac{\partial^4\psi_y}{\partial x\partial y^3} = I_0\frac{\partial^2 U}{\partial t^2}\\ &+ J_1\frac{\partial^2\psi_x}{\partial t^2} - c_1 I_3\frac{\partial^3 W}{\partial x\partial t^2}, \end{aligned} \tag{16}$$

$$\begin{aligned} &B_1\frac{\partial^2 U}{\partial x\partial y} + B_2\frac{\partial^4 U}{\partial x^3\partial y} + B_3\frac{\partial^4 U}{\partial x\partial y^3} + B_4\frac{\partial^3 W}{\partial x^2\partial y} + B_5\frac{\partial^5 W}{\partial x^4\partial y} + B_6\frac{\partial^5 W}{\partial x^2\partial y^3}\\ &+ B_7\frac{\partial^3 W}{\partial y^3} + B_8\frac{\partial^5 W}{\partial y^5} + B_9\frac{\partial^2 V}{\partial y^2} + B_{10}\frac{\partial^2 V}{\partial x^2} + B_{11}\frac{\partial^4 V}{\partial x^2\partial y^2} + B_{12}\frac{\partial^4 V}{\partial y^4}\\ &+ B_{13}\frac{\partial^4 V}{\partial x^4} + B_{14}\frac{\partial^2\psi_x}{\partial x\partial y} + B_{15}\frac{\partial^4\psi_x}{\partial x^3\partial y} + B_{16}\frac{\partial^4\psi_x}{\partial x\partial y^3} + B_{17}\frac{\partial^2\psi_y}{\partial x^2}\\ &+ B_{18}\frac{\partial^2\psi_y}{\partial x^2} + B_{19}\frac{\partial^4\psi_y}{\partial y^4} + B_{20}\frac{\partial^4\psi_y}{\partial x^2\partial y^2} + B_{21}\frac{\partial^4\psi_y}{\partial x^4} = I_0\frac{\partial^2 V}{\partial t^2} + J_1\frac{\partial^2\psi_y}{\partial t^2}\\ &- c_1 I_3\frac{\partial^3 W}{\partial y\partial t^2}, \end{aligned} \tag{17}$$

$$\begin{aligned} &C_1\frac{\partial^5 U}{\partial x^5} + C_2\frac{\partial^3 U}{\partial x^3} + C_3\frac{\partial^5 U}{\partial x^3\partial y^2} + C_4\frac{\partial^3 U}{\partial x\partial y^2} + C_5\frac{\partial^5 U}{\partial x\partial y^4} + C_6\frac{\partial^3 V}{\partial x^2\partial y}\\ &+ C_7\frac{\partial^5 V}{\partial x^2\partial y^3} + C_8\frac{\partial^5 V}{\partial x^4\partial y} + C_9\frac{\partial^3 V}{\partial y^3} + C_{10}\frac{\partial^5 V}{\partial y^5} + C_{11}\frac{\partial^2 W}{\partial x^2}\\ &+ C_{12}\frac{\partial^6 W}{\partial x^6} + C_{13}\frac{\partial^4 W}{\partial x^4} + C_{14}\frac{\partial^4 W}{\partial x^2\partial y^2} + C_{15}\frac{\partial^2 W}{\partial y^2} + C_{16}\frac{\partial^6 W}{\partial y^6}\\ &+ C_{17}\frac{\partial^6 W}{\partial x^4\partial y^2} + C_{18}\frac{\partial^6 W}{\partial x^2\partial y^4} + C_{19}\frac{\partial^4 W}{\partial y^4} + C_{20}\frac{\partial\psi_x}{\partial x} + C_{21}\frac{\partial^3\psi_x}{\partial x^3}\\ &+ C_{22}\frac{\partial^3\psi_x}{\partial x\partial y^2} + C_{23}\frac{\partial^5\psi_x}{\partial x^5} + C_{24}\frac{\partial^5\psi_x}{\partial x^3\partial y^2} + C_{25}\frac{\partial^5\psi_x}{\partial x\partial y^4} + C_{26}\frac{\partial\psi_y}{\partial y}\\ &+ C_{27}\frac{\partial^3\psi_y}{\partial y^3} + C_{28}\frac{\partial^3\psi_y}{\partial x^2\partial y} + C_{29}\frac{\partial^5\psi_y}{\partial x^4\partial y} + C_{30}\frac{\partial^5\psi_y}{\partial x^2\partial y^3} + C_{31}\frac{\partial^5\psi_y}{\partial y^5}\\ &= I_0\frac{\partial^2 W}{\partial t^2} - c_1^2 I_6\left(\frac{\partial^2 W}{\partial x^2\partial t^2} + \frac{\partial^2 W}{\partial y^2\partial t^2}\right) + c_1 I_3\left(\frac{\partial^3 U}{\partial x\partial t^2} + \frac{\partial^3 V}{\partial y\partial t^2}\right)\\ &+ c_1 J_4\left(\frac{\partial^3\psi_x}{\partial x\partial t^2} + \frac{\partial^3\psi_y}{\partial y\partial t^2}\right) \end{aligned} \tag{18}$$

$$D_1\frac{\partial^2 U}{\partial x^2}+D_2\frac{\partial^4 U}{\partial x^4}+D_3\frac{\partial^4 U}{\partial x^2\partial\theta^2}+D_4\frac{\partial^2 U}{\partial y^2}+D_5\frac{\partial^4 U}{\partial y^4}+D_6\frac{\partial^2 V}{\partial x\partial y}+D_7\frac{\partial^2 V}{\partial x^3\partial y}+D_8\frac{\partial^4 V}{\partial x\partial y^3}+D_9\frac{\partial^5 W}{\partial x^5}+D_{10}\frac{\partial^3 W}{\partial x\partial y^2}+D_{11}\frac{\partial^3 W}{\partial x^3}+D_{12}\frac{\partial^5 W}{\partial x^3\partial y^2}+D_{13}\frac{\partial^5 W}{\partial x\partial y^4}+D_{14}\frac{\partial^2\psi_x}{\partial x^2}+D_{15}\frac{\partial^4\psi_x}{\partial x^4}+D_{16}\frac{\partial^4\psi_x}{\partial x^2\partial y^2}+D_{17}\frac{\partial^2\psi_x}{\partial y^2}+D_{18}\frac{\partial^2\psi_y}{\partial x\partial y}+D_{19}\frac{\partial^4\psi_x}{\partial y^4}+D_{20}\frac{\partial^4\psi_y}{\partial x^3\partial y}+D_{21}\frac{\partial^4\psi_y}{\partial x\partial y^3}+D_{22}\psi_x+D_{23}\frac{\partial W}{\partial x}=J_1\frac{\partial^2 U}{\partial t^2}+K_2\frac{\partial^2\psi_x}{\partial t^2}-c_1J_4\frac{\partial^3 W}{\partial x\partial t^2}, \tag{19}$$

$$E_1\frac{\partial^2 U}{\partial x\partial y}+E_2\frac{\partial^4 U}{\partial x^3\partial y}+E_3\frac{\partial^4 U}{\partial x\partial y^3}+E_4\frac{\partial^3 W}{\partial x^2\partial y}+E_5\frac{\partial^5 W}{\partial x^4\partial y}+E_6\frac{\partial^5 W}{\partial x^2\partial y^3}+E_7\frac{\partial^3 W}{\partial y^3}+E_8\frac{\partial^5 W}{\partial y^5}+E_9\frac{\partial^2 V}{\partial y^2}+E_{10}\frac{\partial^2 V}{\partial x^2}+E_{11}\frac{\partial^4 V}{\partial x^2\partial y^2}+E_{12}\frac{\partial^4 V}{\partial y^4}+E_{13}\frac{\partial^4 V}{\partial x^4}+E_{14}\frac{\partial^2\psi_x}{\partial x\partial y}+E_{15}\frac{\partial^4\psi_x}{\partial x^3\partial y}+E_{16}\frac{\partial^4\psi_x}{\partial x\partial y^3}+E_{17}\frac{\partial^2\psi_y}{\partial x^2}+E_{18}\frac{\partial^2\psi_y}{\partial x^2}+E_{19}\frac{\partial^4\psi_y}{\partial y^4}+E_{20}\frac{\partial^4\psi_y}{\partial x^2\partial y^2}+E_{21}\frac{\partial^4\psi_y}{\partial x^4}+E_{22}\psi_y+E_{23}\frac{\partial W}{\partial y}=J_1\frac{\partial^2 V}{\partial t^2}+K_2\frac{\partial^2\psi_x}{\partial t^2}-c_1J_4\frac{\partial^3 W}{\partial y\partial t^2}. \tag{20}$$

Coefficients A, B, C, D and E in Eqs. (16)–(20) are contained in Appendix A, and c_1, K, J and I are as follows:

$$I_i=\int_{-h/2}^{h/2}(\rho(z))^i dz, J_i=I_i-c_1I_{i+2},\quad K_2=I_2-2c_1I_4+c_1^2I_6, c_1=4/3h^2. \tag{21}$$

Afterwards, the free vibrations of a simply supported FG-CNTRC nanoplate are studied. The effects of different parameters such as size parameter and volume fraction of the CNTs and the manner of distribution of CNTs in the FG-CNTRC nanoplates are determined using Mindlin's strain gradient theory and the results are compared to those of the classical theory.

To solve the above-mentioned equations, the FG-CNTRC nanoplate is considered to be simply supported., In this regard, the boundary conditions of the composite nanoplate are divided into two categories including classical boundary conditions and as well as higher order ones. The classical boundary conditions are expressed as:

$$V=0,\quad W=0,\quad \psi_y=0,\quad N_x=0,\quad M_x=0.\quad x=0,a,$$
$$U=0,\quad W=0,\quad \psi_x=0,\quad N_y=0,\quad M_y=0.\quad y=0,b. \tag{22}$$

Given that FG-CNTRC nanoplate displacements have been considered in the three u, v, and w directions, higher order boundary conditions demand complicated computations. For instance, Papargyri-Beskou et al. developed the higher order boundary conditions and equations of a nanoplate in which displacement occurred only along w, which was indicative of the sheer size and complexity of the computations [30]. For this reason, in the present paper, in order to solve vibration problem of FG-CNTRC nanoplate based on classical boundary conditions and Navier solution, the displacements are expressed similar to those reported in [31]:

$$\begin{aligned}
U(x,y,t)&=\sum_n\sum_m U_0\cos\left(\frac{m\pi x}{a}\right)\sin\left(\frac{n\pi y}{b}\right),\\
V(x,y,t)&=\sum_n\sum_m V_0\sin\left(\frac{m\pi x}{a}\right)\cos\left(\frac{n\pi y}{b}\right),\\
W(x,y,t)&=\sum_n\sum_m W_0\sin\left(\frac{m\pi x}{a}\right)\sin\left(\frac{n\pi y}{b}\right),\\
\psi_x(x,y,t)&=\sum_n\sum_m \Psi_x\cos\left(\frac{m\pi x}{a}\right)\sin\left(\frac{n\pi y}{b}\right),\\
\psi_y(x,y,t)&=\sum_n\sum_m \Psi_y\sin\left(\frac{m\pi x}{a}\right)\cos\left(\frac{n\pi y}{b}\right),
\end{aligned} \tag{23}$$

By substituting Eq. (23) into Eqs. (16)–(20), the equations are written in matrix form as:

$$[K]\{d\}+[M]\left\{\ddot{d}\right\}=0, \tag{24}$$

where

$$\{d\}=\{d_0\}e^{\omega t}. \tag{25}$$

By substituting Eq. (25) into Eq. (24), the equations are written as:

$$([K]+\omega^2[M])\{d_0\}=0, \tag{26}$$

where the coefficient $\{d_0\}^T=\{U_0V_0W_0\Psi_x\Psi_y\}^T$ is related to the domain of frequency modes and ω is the natural frequency of the FG-CNTRC nanoplate. In order for the problem to have non-trivial solutions, the determinant of the matrix of coefficient must be zero.

3. Result and discussions

In Sections 3.1–3.4, the mechanical properties of the CNT and the polymer matrix are considered as follows:

$$E_{11}^{CNT}=5.6466\ \text{Tpa},\quad E_{22}^{CNT}=7.0800\ \text{Tpa},\quad G_{12}^{CNT}=1.9445\ \text{Tpa},\quad \upsilon_{12}^{CNT}=0.175. \tag{27}$$

$$\rho^{CNT}=1.4\ \text{g/cm}^3,\quad E^m=2.1\ \text{Gpa},\quad \upsilon^m=0.34,\quad \rho^m=1.15\ \text{g/cm}^3,\quad \eta_3=\eta_2. \tag{28}$$

$$\bar{V}_{CNT}=0.11\rightarrow\eta_1=0.149,\quad \eta_2=0.934,\quad \bar{V}_{CNT}=0.14\rightarrow\eta_1=0.150,\quad \eta_2=0.941,\quad \bar{V}_{CNT}=0.17\rightarrow\eta_1=0.149,\quad \eta_2=1.381. \tag{29}$$

Also, the natural frequency has been rendered dimensionless as $\Omega=\omega h\sqrt{\rho^m/E^m}$.

3.1. Comparison of results with other references

To evaluate the results more efficiently, the natural frequencies for the classical theory have been compared to those in Ref. [17]. In this reference, the FSDT theory has been used and the equations have been solved using the FEM method. Also, the natural frequency has been rendered dimensionless as $\Omega=\omega(a^2/h)\sqrt{\rho^m/E^m}$. Based on the results presented in the table, the results of this paper have high consistency with those of Ref. [17]. The results drawn by using the TSDT are also presented in the table. The frequency values determined by TSDT are lower than those by FSDT. That is because (a) in the FSDT, the shear correction factor is used to correct the assumption of fixity of transverse shear strains where there is no need to correction in the TSDT, and (b) displacement is assumed to be smaller in the TSDT than in the FSDT theory and the presence of higher order shear and moments increases FG-CNTRC nanoplate rigidity in the TSDT. Therefore,

Table 1
Natural frequency of FG-CNTRC nanoplate.

$\bar{V}_{CNT}$	b/h	n	UD			FG-O			FG-X		
			FSDT [21]	FSDT present study	TSDT present study	FSDT [21]	FSDT present study	TSDT present study	FSDT [21]	FSDT present study	TSDT present study
0.11	10	1	13.532	13.510	13.555	11.550	11.456	11.466	14.616	14.625	14.728
		2	17.700	17.682	17.722	16.265	16.057	16.065	18.646	18.713	18.781
	20	1	17.355	17.304	17.310	13.532	13.391	13.406	19.939	19.927	19.961
		2	21.511	21.415	21.421	18.486	18.137	18.152	23.736	23.816	23.839
0.14	10	1	14.306	14.316	14.381	12.338	12.285	12.302	15.368	15.405	15.465
		2	18.362	18.410	18.466	16.848	16.714	16.732	19.385	19.508	19.537
	20	1	18.921	18.923	18.933	14.784	14.705	14.381	21.642	21.655	21.674
		2	22.867	22.880	22.890	19.462	19.216	19.251	25.359	25.480	25.491
0.17	10	1	16.815	16.783	16.837	14.282	14.167	14.182	18.278	18.280	18.291
		2	22.063	22.038	22.085	20.091	19.835	20.034	23.541	23.608	23.612
	20	1	21.456	21.388	21.395	16.628	16.469	16.594	24.764	24.736	24.761
		2	26.706	26.579	26.587	22.739	22.318	22.573	29.819	29.836	29.842

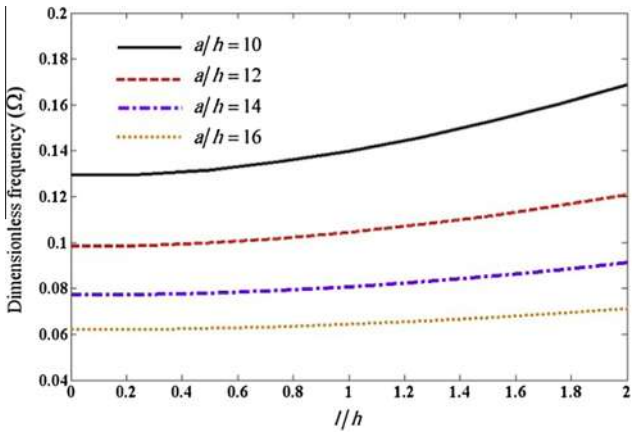

Fig. 2. CNTRC nanoplate natural frequency based on size parameter in different a/h ratios and UD.

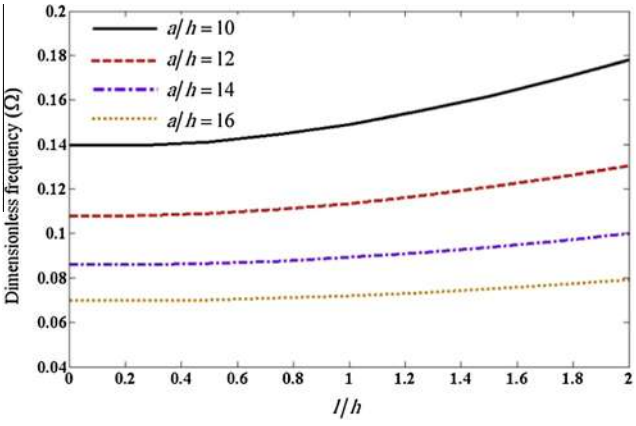

Fig. 3. CNTRC nanoplate natural frequency based on size parameter in different a/h ratios and FG-O.

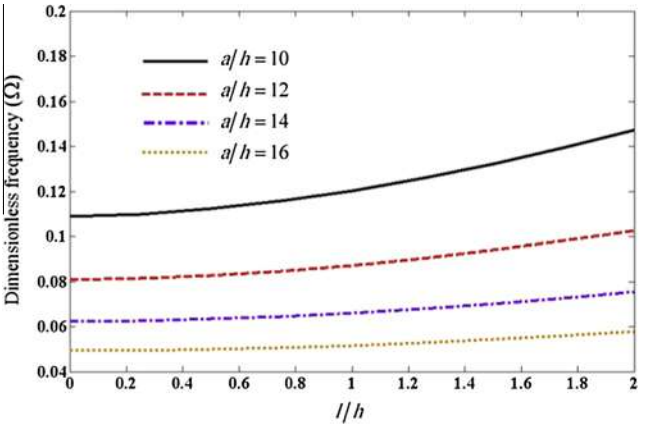

Fig. 4. CNTRC nanoplate natural frequency based on size parameter in different a/h ratios and FG-X.

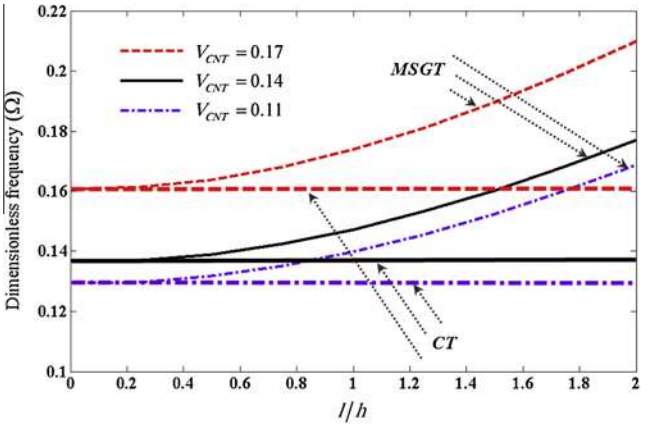

Fig. 5. CNTRC nanoplate natural frequency based on size parameter in different $\bar{V}_{CNT}$ and UD.

plate deformation is greater in the FSDT and therefore, the frequencies are smaller[32] (see Table 1).

3.2. Effect of size parameter

Figs. 2–4 display the natural frequency of the FG-CNTRC nanoplate based on size parameter in different dimensions. This section considers ($a/b = 1$). Increase in the size parameter of FG-CNRTC nanoplate is accompanied by increase in its natural frequency, which is due to the increase in nanoplate rigidity. Moreover, increase in the dimensions of the FG-CNTRC nanoplate results in decrease in its frequencies. In fact, an increase in nanoplate dimensions is accompanied by a decrease in its rigidity. Besides, in these illustrations, the effect of distribution of CNTs in nanoplates has been investigated. The frequency values obtained in FG-O nanoplate are higher than those in FG-X and UD nanoplates. In fact, the FG-O nanoplate has greater rigidity.

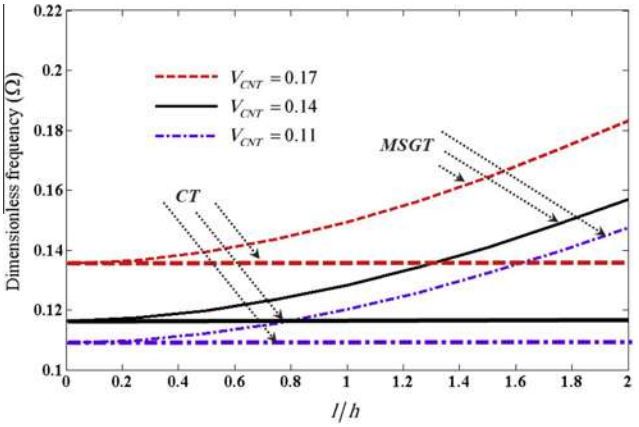

Fig. 6. CNTRC nanoplate natural frequency based on size parameter in different $\bar{V}_{CNT}$ and FG-O.

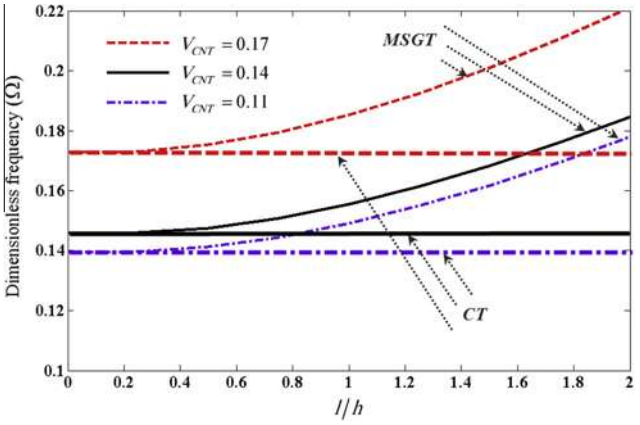

Fig. 7. CNTRC nanoplate natural frequency based on size parameter in different $\bar{V}_{CNT}$ and FG-X.

3.3. Effect of volume fraction of CNTs

Figs. 5–7, present the natural frequency of the CNTs of the CNTRC nanoplate based on the size parameter and different volume fractions of CNTs. This section considers $(a/b = 1)$ and $(a/h = 10)$. Increase in the volume fraction of CNTs in CNTRC nanoplate is accompanied by increase in its natural frequency, which is due to CNT rigidity. Besides, natural frequency increase in Mindlin's strain gradient theory is higher than that in the classical theory, which is indicative of the prediction of greater stiffness by Mindlin's strain gradient theory as compared to the classical theory. This is qualitatively consistent with the results presented by the references. These results have been obtained for the three FG-O, FG-X and UD nanoplates.

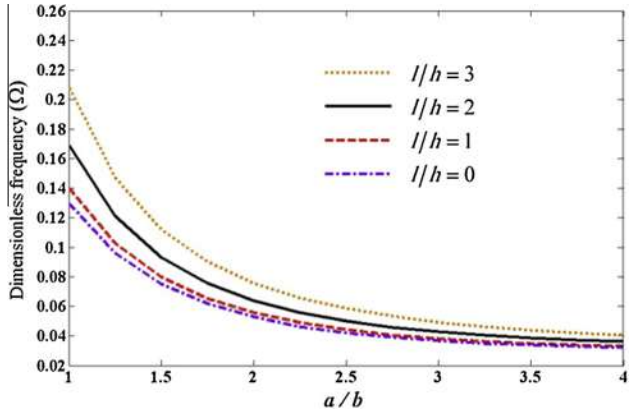

Fig. 8. CNTRC nanoplate natural frequency based on a/b ratio and size parameter in $\bar{V}_{CNT} = 0.11$.

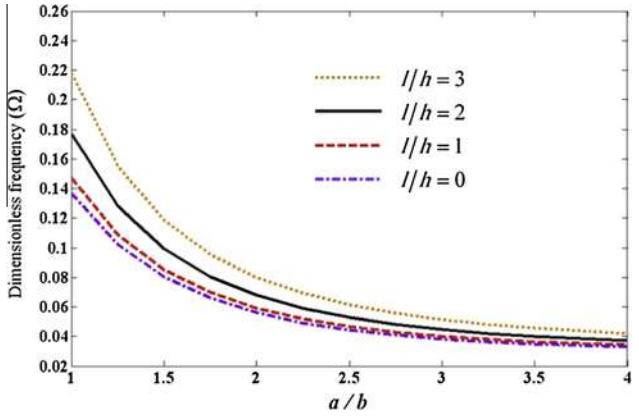

Fig. 9. CNTRC nanoplate natural frequency based on a/b ratio and size parameter in $\bar{V}_{CNT} = 0.14$.

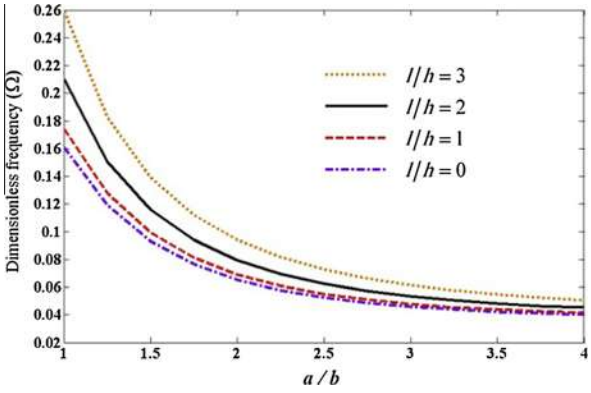

Fig. 10. CNTRC nanoplate natural frequency based on a/b ratio and size parameter in $\bar{V}_{CNT} = 0.17$.

3.4. Effect of ratio of nanoplate dimensions

Figs. 8–10 display the natural frequency of CNTRC nanoplate based on nanoplate dimensions, size parameter, and different volume fractions of CNTs. This section considers UD nanoplate and $(a/h = 10)$. Increase in a/b ratio leads to decrease in CNT natural frequency. Also, increase in a/b ratio leads to decrease in the size parameter. Of course, it should be noted that in the CNTRC nanoplate model with Mindlin's strain gradient theory, the effect of size parameter affects the a/b ratio, and the degree of the size parameter is determined by the degree of dimensions and thickness, and this parameter has greater effect in CNTRC nanoplates with shorter dimensions; and increase in the dimension of CNTRC nanoplate reduces its effect due to the nature of the CNTRC nanoplate. According to Figs. 8–10, an increase in the volume fraction of CNTs leads to an increase in the natural frequency difference in different dimensions, which is indicative of an increase in the rigidity of CNTRC nanoplate in high volume fractions of CNTs.

4. Conclusion

In this paper, equations of the FG-CNTRC nanoplate were derived using TSDT and Mindlin's strain gradient theory. Using Hamilton's principle, this non-classical formulation which incorporates the size parameter was obtained. Afterwards, the free vibration of FG-CNTRC nanoplate was investigated, and natural frequencies for different parameters such as size parameter, FG-CNTRC nanoplate dimensions, and different volume fractions were examined and compared with the classical theory. Moreover, to conduct a more efficient evaluation, a case studied previously by the references was solved using the classical theory and its natural frequency were analyzed, indicating the general accuracy and authenticity of the results. The results reveal that an increase in the size parameter and volume fraction of the CNT and a decrease in the FG-CNTRC nanoplate dimensions lead to an increase in the frequency of the FG-CNTRC nanoplate. Moreover, in smaller dimensions of the FG-CNTRC nanoplate, the size parameter has a greater effect on the natural frequency.

Appendix A

In equations of motion (16)–(20), the constant coefficients A_i, B_i, C_i, D_i and E_i are rewritten as follows:

$$A_i = \int_{-h/2}^{h/2} \bar{A}_i(z)dz, \tag{A.1}$$

$$B_i = \int_{-h/2}^{h/2} \bar{B}_i(z)dz, \tag{A.2}$$

$$C_i = \int_{-h/2}^{h/2} \bar{C}_i(z)dz, \tag{A.3}$$

$$D_i = \int_{-h/2}^{h/2} \bar{D}_i(z)dz, \tag{A.4}$$

$$E_i = \int_{-h/2}^{h/2} \bar{E}_i(z)dz, \tag{A.5}$$

In equations of motion (A.1)–(A.5), the constant coefficients $\bar{A}_i$, $\bar{B}_i$, $\bar{C}_i$, $\bar{D}_i$ and $\bar{E}_i$ are rewritten as follows:

$$\begin{aligned}
&\bar{A}_1 = Q_{11},\ \bar{A}_2 = -l^2Q_{11},\ \bar{A}_3 = -l^2(Q_{11}+Q_{33}),\ \bar{A}_4 = Q_{33},\\
&\bar{A}_5 = -l^2Q_{33},\ \bar{A}_6 = Q_{12}+Q_{33},\ \bar{A}_7 = -l^2(Q_{12}+Q_{33}),\\
&\bar{A}_8 = -l^2(Q_{12}+Q_{33}),\ \bar{A}_9 = c_1z^3l^2Q_{11},\ \bar{A}_{10} = c_1(-z^3+6zl^2)(Q_{12}+2Q_{33}),\\
&\bar{A}_{11} = c_1z^3l^2(Q_{11}+Q_{12}+2Q_{33}),\ \bar{A}_{12} = c_1(-z^3+6zl^2)Q_{11},\\
&\bar{A}_{13} = c_1z^3l^2(Q_{12}+2Q_{33}),\ \bar{A}_{14} = (z-c_1z^3+6c_1zl^2)Q_{11},\\
&\bar{A}_{15} = -l^2(z-c_1z^3)Q_{11},\ \bar{A}_{16} = -l^2(z-c_1z^3)(Q_{11}+Q_{33}),\\
&\bar{A}_{17} = (z-c_1z^3+6c_1zl^2)Q_{33},\ \bar{A}_{18} = (z-c_1z^3+6c_1zl^2)(Q_{12}+Q_{33}),\\
&\bar{A}_{19} = -l^2(z-c_1z^3)Q_{33},\ \bar{A}_{20} = -l^2(z-c_1z^3)(Q_{12}+Q_{33}),\\
&\bar{A}_{21} = -l^2(z-c_1z^3)(Q_{11}+Q_{33}).
\end{aligned} \tag{A.6}$$

$$\begin{aligned}
&\bar{B}_1 = Q_{12}+Q_{33},\ \bar{B}_2 = -l^2(Q_{12}+Q_{33}),\ \bar{B}_3 = -l^2(Q_{12}+Q_{33}),\\
&\bar{B}_4 = c_1(-z^3+6zl^2)(Q_{12}+2Q_{33}),\ \bar{B}_5 = c_1z^3l^2(Q_{12}+2Q_{33}),\\
&\bar{B}_6 = c_1z^3l^2(Q_{11}+Q_{22}+2Q_{33}),\ \bar{B}_7 = c_1(-z^3+6zl^2)Q_{22},\\
&\bar{B}_8 = c_1z^3l^2Q_{22},\ \bar{B}_9 = Q_{22},\ \bar{B}_{10} = Q_{33},\ \bar{B}_{11} = -l^2(Q_{22}+Q_{33}),\\
&\bar{B}_{12} = -l^2Q_{22},\ \bar{B}_{13} = -l^2Q_{33},\ \bar{B}_{14} = (z-c_1z^3+6c_1zl^2)(Q_{12}+Q_{33}),\\
&\bar{B}_{15} = -l^2(z-c_1z^3)(Q_{12}+Q_{33}),\ \bar{B}_{16} = -l^2(z-c_1z^3)(Q_{12}+Q_{33}),\\
&\bar{B}_{17} = (z-c_1z^3+6c_1zl^2)Q_{33},\ \bar{B}_{18} = (z-c_1z^3+6c_1zl^2)Q_{22},\\
&\bar{B}_{19} = -l^2(z-c_1z^3)Q_{22},\ \bar{B}_{20} = -l^2(z-c_1z^3)(Q_{22}+Q_{33}),\\
&\bar{B}_{21} = -l^2(z-c_1z^3)Q_{33}.
\end{aligned} \tag{A.7}$$

$$\begin{aligned}
&\bar{C}_1 = -c_1z^3l^2Q_{11},\ \bar{C}_2 = c_1z^3Q_{11},\ \bar{C}_3 = -c_1z^3l^2(Q_{11}+Q_{12}+2Q_{33}),\\
&\bar{C}_4 = c_1z^3(Q_{12}+Q_{33}),\ \bar{C}_5 = -c_1z^3l^2(Q_{12}+Q_{33}),\\
&\bar{C}_6 = c_1z^3(Q_{12}+Q_{33}),\ \bar{C}_7 = -c_1z^3l^2(Q_{12}+Q_{22}+Q_{33}),\\
&\bar{C}_8 = -c_1z^3l^2(Q_{12}+Q_{33}),\ \bar{C}_9 = c_1z^3Q_{22},\ \bar{C}_{10} = -c_1z^3l^2Q_{22},\\
&\bar{C}_{11} = (1-3c_1z^2+6c_1l^2)(1-c_2z^2)Q_{44},\ \bar{C}_{12} = c_1^2z^3l^2Q_{11},\\
&\bar{C}_{13} = -l^2(1-3c_1z^2)(1-c_2z^2)Q_{44}+c_1z^3(-c_1z^3+6c_1zl^2)Q_{11},\\
&\bar{C}_{14} = -l^2(1-3c_1z^2)(1-c_2z^2)(Q_{44}+Q_{55})\\
&\qquad +2c_1z^3(-c_1z^3+6c_1zl^2)(Q_{12}+Q_{33}),\\
&\bar{C}_{15} = (1-3c_1z^2+6c_1l^2)(1-c_2z^2)Q_{55},\\
&\bar{C}_{16} = c_1^2z^6l^2Q_{22},\ \bar{C}_{17} = c_1z^6l^2(-Q_{11}+2Q_{12}+2Q_{33}),\\
&\bar{C}_{18} = c_1z^6l^2(2Q_{12}+Q_{22}+2Q_{33}),\ \bar{C}_{19} = -l^2(1-3c_1z^2)(1-c_2z^2)Q_{55}\\
&\qquad +c_1z^3(-c_1z^3+6c_1zl^2)Q_{22},\ \bar{C}_{20} = (1-3c_1z^2+6c_1l^2)(1-c_2z^2)Q_{44},\\
&\bar{C}_{21} = -l^2(1-3c_1z^2)(1-c_2z^2)Q_{44}+c_1z^3(z-c_1z^3+6c_1zl^2)Q_{11},\\
&\bar{C}_{22} = -l^2(1-3c_1z^2)(1-c_2z^2)Q_{44}+c_1z^3(z-c_1z^3+6c_1zl^2)(Q_{12}+Q_{33}),\\
&\bar{C}_{23} = -c_1z^4l^2(1-c_1z^2)Q_{11},\ \bar{C}_{24} = -c_1z^4l^2(1-c_1z^2)(Q_{11}+Q_{12}+Q_{33}),\\
&\bar{C}_{25} = -c_1z^4l^2(1-c_1z^2)(Q_{12}+Q_{33}),\\
&\bar{C}_{26} = (1-3c_1z^2+6c_1l^2)(1-c_2z^2)Q_{55},\\
&\bar{C}_{27} = -l^2(1-3c_1z^2)(1-c_2z^2)Q_{55}+c_1z^3(z-c_1z^3+6c_1zl^2)(Q_{22}),\\
&\bar{C}_{28} = -l^2(1-3c_1z^2)(1-c_2z^2)Q_{44}+c_1z^3(z-c_1z^3+6c_1zl^2)(Q_{12}+Q_{33}),\\
&\bar{C}_{29} = -c_1z^4l^2(1-c_1z^2)(Q_{12}+Q_{33}),\\
&\bar{C}_{30} = -c_1z^4l^2(1-c_1z^2)(Q_{12}+Q_{22}+Q_{33}),\ \bar{C}_{31} = -c_1z^4l^2(1-c_1z^2)Q_{12},
\end{aligned} \tag{A.8}$$

$$\begin{aligned}
&\bar{D}_1 = z(1-c_1z^2)Q_{11},\quad \bar{D}_2 = -z(1-c_1z^2)l^2Q_{11},\\
&\bar{D}_3 = -z(1-c_1z^2)l^2(Q_{11}+Q_{33}),\quad \bar{D}_4 = (1-c_1z^2)zQ_{33},\\
&\bar{D}_5 = -(1-c_1z^2)zl^2Q_{33},\quad \bar{D}_6 = z(1-c_1z^2)(Q_{12}+Q_{33}),\\
&\bar{D}_7 = -z(1-c_1z^2)l^2(Q_{12}+Q_{33}),\quad \bar{D}_8 = -z(1-c_1z^2)l^2(Q_{12}+Q_{33}),\\
&\bar{D}_9 = c_1z^4(1-c_1z^2)l^2Q_{11},\\
&\bar{D}_{10} = c_1z(1-c_1z^2)(-z^3+6zl^2)(Q_{12}+2Q_{33}),\\
&\bar{D}_{11} = c_1z^4l^2(1-c_1z^2)(Q_{11}+Q_{12}+2Q_{33}),\\
&\bar{D}_{12} = c_1(1-c_1z^2)(-z^4+6z^2l^2)Q_{11},\\
&\bar{D}_{13} = c_1z^4l^2(1-c_1z^2)(Q_{12}+2Q_{33}),\\
&\bar{D}_{14} = z^2(1-c_1z^2)(1-c_1z^2+6c_1l^2)Q_{11},\\
&\bar{D}_{15} = -z^2l^2(1-c_1z^2)^2Q_{11},\quad \bar{D}_{16} = -z^2l^2(1-c_1z^2)^2(Q_{11}+Q_{33}),\\
&\bar{D}_{17} = z^2(1-c_1z^2)(1-c_1z^2+6c_1l^2)Q_{33},\\
&\bar{D}_{18} = z^2(1-c_1z^2)(1-c_1z^2+6c_1l^2)(Q_{12}+Q_{33}),\\
&\bar{D}_{19} = -z^2l^2(1-c_1z^2)(1-c_1z^2)Q_{33},\\
&\bar{D}_{20} = -z^2l^2(1-c_1z^2)(1-c_1z^2)(Q_{12}+Q_{33}),\\
&\bar{D}_{21} = -z^2l^2(1-c_1z^2)^2(Q_{11}+Q_{33}),\\
&\bar{D}_{22} = -(1-3c_1z^2+6c_1l^2)(1-c_2z^2)Q_{44},\\
&\bar{D}_{22} = -(1-3c_1z^2+6c_1l^2)(1-c_2z^2)Q_{44},
\end{aligned} \tag{A.9}$$

$$\bar{E}_1 = z(1-c_1z^2)(Q_{12}+Q_{33}),\ \ \bar{E}_2 = -zl^2(1-c_1z^2)(Q_{12}+Q_{33}),$$
$$\bar{E}_3 = -zl^2(1-c_1z^2)(Q_{12}+Q_{33}),$$
$$\bar{E}_4 = c_1z^2(1-c_1z^2)(-z^2+6l^2)(Q_{12}+2Q_{33}),$$
$$\bar{E}_5 = c_1z^4l^2(1-c_1z^2)(Q_{12}+2Q_{33}),$$
$$\bar{E}_6 = c_1z^4l^2(1-c_1z^2)(Q_{11}+Q_{22}+2Q_{33}),$$
$$\bar{E}_7 = c_1z^2(1-c_1z^2)(-z^2+6l^2)Q_{22},\ \ E_8 = c_1z^4l^2(1-c_1z^2)Q_{22},$$
$$\bar{E}_9 = z(1-c_1z^2)Q_{22},\ \ \bar{E}_{10} = z(1-c_1z^2)Q_{33},$$
$$\bar{E}_{11} = -zl^2(1-c_1z^2)(Q_{22}+Q_{33}),\ \ \bar{E}_{12} = -zl^2(1-c_1z^2)Q_{22},$$
$$\bar{E}_{13} = -zl^2(1-c_1z^2)Q_{33},\ \ \bar{E}_{14} = z^2(1-c_1z^2)(1-c_1z^2+6c_1l^2)(Q_{12}+Q_{33}),$$
$$\bar{E}_{15} = -z^2l^2(1-c_1z^2)^2(Q_{12}+Q_{33}),\ \ \bar{E}_{16} = -z^2l^2(1-c_1z^2)^2(Q_{12}+Q_{33}),$$
$$\bar{E}_{17} = z^2(1-c_1z^2)(1-c_1z^2+6c_1l^2)Q_{33},$$
$$\bar{E}_{18} = z^2(1-c_1z^2)(1-c_1z^2+6c_1l^2)Q_{22},$$
$$\bar{E}_{19} = -z^2l^2(1-c_1z^2)^2Q_{22},\ \ \bar{E}_{20} = -z^2l^2(1-c_1z^2)^2(Q_{22}+Q_{33}),$$
$$\bar{E}_{21} = -z^2l^2(1-c_1z^2)^2Q_{33},\ \ \bar{E}_{22} = -(1-3c_1z^2+6c_1l^2)(1-c_2z^2)Q_{55},$$
$$\bar{E}_{23} = -(1-3c_1z^2+6c_1l^2)(1-c_2z^2)Q_{55}. \qquad (A.10)$$

References

[1] Esawi AM, Farag MM. Polymer nanotube composites: latest challenges and applications. Polymer nanotubes nanocomposites: synthesis, properties and applications; 2014:429.
[2] Fiedler B, Gojny FH, Wichmann MH, Nolte M, Schulte K. Fundamental aspects of nano-reinforced composites. Compos Sci Technol 2006;66:3115–25.
[3] Ansari R, Gholami R, Rouhi H. Vibration analysis of single-walled carbon nanotubes using different gradient elasticity theories. Compos Part B 2012;43:2985–9.
[4] Ansari R, Gholami R, Rouhi H. Various gradient elasticity theories in predicting vibrational response of single-walled carbon nanotubes with arbitrary boundary conditions. J Vib Control 2013;19:708–19.
[5] Eringen AC, Edelen D. On nonlocal elasticity. Int J Eng Sci 1972;10:233–48.
[6] Eringen AC. On differential equations of nonlocal elasticity and solutions of screw dislocation and surface waves. J Appl Phys 1983;54:4703–10.
[7] Reddy J. Nonlocal theories for bending, buckling and vibration of beams. Int J Eng Sci 2007;45:288–307.
[8] Reddy J. Nonlocal nonlinear formulations for bending of classical and shear deformation theories of beams and plates. Int J Eng Sci 2010;48:1507–18.
[9] Babaei H, Shahidi A. Small-scale effects on the buckling of quadrilateral nanoplates based on nonlocal elasticity theory using the Galerkin method. Arch Appl Mech 2011;81:1051–62.
[10] Roque C, Ferreira A, Reddy J. Analysis of Timoshenko nanobeams with a nonlocal formulation and meshless method. Int J Eng Sci 2011;49:976–84.
[11] Zeighampour H, Tadi Beni Y. Cylindrical thin-shell model based on modified strain gradient theory. Int J Eng Sci 2014;78:27–47.
[12] Zeighampour H, Tadi Beni Y. Analysis of conical shells in the framework of coupled stresses theory. Int J Eng Sci 2014;81:107–22.
[13] Akgöz B, Civalek Ö. Free vibration analysis of axially functionally graded tapered Bernoulli–Euler microbeams based on the modified couple stress theory. Compos Struct 2013;98:314–22.
[14] Zeighampour H, Beni YT. A shear deformable cylindrical shell model based on couple stress theory. Arch Appl Mech 2014:1–15.
[15] Ke L-L, Yang J, Kitipornchai S. Nonlinear free vibration of functionally graded carbon nanotube-reinforced composite beams. Compos Struct 2010;92:676–83.
[16] Yas M, Samadi N. Free vibrations and buckling analysis of carbon nanotube-reinforced composite Timoshenko beams on elastic foundation. Int J Press Vessels Pip 2012;98:119–28.
[17] Shen H-S. Nonlinear bending of functionally graded carbon nanotube-reinforced composite plates in thermal environments. Compos Struct 2009;91:9–19.
[18] Lei ZX, Liew KM, Yu JL. Large deflection analysis of functionally graded carbon nanotube-reinforced composite plates by the element-free kp-Ritz method. Comput Methods Appl Mech Eng 2013;256:189–99.
[19] Lei Z, Liew KM, Yu J. Buckling analysis of functionally graded carbon nanotube-reinforced composite plates using the element-free< i> kp</i>-Ritz method. Compos Struct 2013;98:160–8.
[20] Alibeigloo A. Static analysis of functionally graded carbon nanotube-reinforced composite plate embedded in piezoelectric layers by using theory of elasticity. Compos Struct 2013;95:612–22.
[21] Zhu P, Lei Z, Liew KM. Static and free vibration analyses of carbon nanotube-reinforced composite plates using finite element method with first order shear deformation plate theory. Compos Struct 2012;94:1450–60.
[22] Abdollahzadeh Shahrbabaki E, Alibeigloo A. Three-dimensional free vibration of carbon nanotube-reinforced composite plates with various boundary conditions using Ritz method. Compos Struct 2014;111:362–70.
[23] Toupin RA. Elastic materials with couple-stresses. Arch Ration Mech Anal 1962;11:385–414.
[24] Mindlin RD, Tiersten HF. Effects of couple-stresses in linear elasticity. Arch Ration Mech Anal 1962;11:415–48.
[25] Koiter WT. Couple stresses in the theory of elasticity: I and II. Proc K Ned Akad Wet 1964;67:17–44.
[26] Mindlin RD. Micro-structure in linear elasticity. Arch Ration Mech Anal 1964;16:51–78.
[27] Mindlin RD. Second gradient of strain and surface-tension in linear elasticity. Int J Solids Struct 1965;1:417–38.
[28] Aifantis EC. On the role of gradients in the localization of deformation and fracture. Int J Eng Sci 1992;30:1279–99.
[29] Wang C, Reddy JN, Lee K. Shear deformable beams and plates: relationships with classical solutions. Elsevier; 2000.
[30] Papargyri-Beskou S, Giannakopoulos AE, Beskos DE. Variational analysis of gradient elastic flexural plates under static loading. Int J Solids Struct 2010;47:2755–66.
[31] Sahmani S, Ansari R. On the free vibration response of functionally graded higher-order shear deformable microplates based on the strain gradient elasticity theory. Compos Struct 2013;95:430–42.
[32] Shufrin I, Eisenberger M. Stability and vibration of shear deformable plates––first order and higher order analyses. Int J Solids Struct 2005;42:1225–51.